Contents lists available at CEPM

Computational Engineering and Physical Modeling

Journal homepage: www.jcepm.com

3D Semi-Analytical Solutions for Functionally Grade Power Law Varied Laminate Subjected to Thermo-Mechanical Loading

S. P. Kulkarni[1*], **S. S. Pendhari**[2]

1. Research Scholar, Structural Engineering Department, Veermata Jijabai Technological Institute, Matunga, Mumbai 400 019, India
2. Associate Professor, Structural Engineering Department, Veermata Jijabai Technological Institute, Matunga, Mumbai 400 019, India

Corresponding author: sspendhari@st.vjti.ac.in

https://doi.org/10.22115/CEPM.2021.265578.1148

ARTICLE INFO

Article history:
Received: 03 January 2021
Revised: 28 April 2021
Accepted: 22 November 2021

Keywords:
BVP;
Power law;
3D laminate;
FGM.

ABSTRACT

This paper describes formulation for calculation of actual through thickness temperature variation followed by stress and displacement analysis of all-around simply supported functionally graded (FG) laminate using a semi-analytical approach. This approach has depended on a two-point boundary value problem (BVP) governed by first-order ordinary differential equations (ODEs). Developed formulation carries the advantage of both elasticity solution as well as ESL or approximate theories. This new model capable of providing accurate results without any approximation along the thickness of FG laminate. Material properties like heat conductivity, modulus of elasticity and thermal expansion coefficient are considered to be varied by a power law. The numerical investigation has been performed to examine thermal loading response on the FGM laminate and transverse loading applied on the laminate's top surface. The results are obtained for two types of thermal loading, obtained by heat conduction formulation received by developed semi-analytical approach and another with assumed power law variation and compared with each other. Leads outcomes from parametric studies, which will be helpful for further research in this area.

How to cite this article: Kulkarni, S. P., & Pendhari, S. S. (2021). 3D Semi-Analytical Solutions for Functionally Grade Power Law Varied Laminate Subjected to Thermo-Mechanical Loading. Computational Engineering and Physical Modeling, 4(3), 70–98. https://doi.org/10.22115/cepm.2021.265578.1148

1. Introduction

Layered composite materials are extensively used in the automotive industry due to their significant characteristics like high stiffness, long fatigue life, wear resistance, strength to weight ratio, etc. These layered composite materials are subjected to residual stress concentration, matrix cracking, delamination etc., problems. For avoiding these problems, a modern class of materials/stuff has been invented called functionally graded material (FGM), generally made up of ceramic on one side and metal on another side. This FGM act as a barrier between high temperature and low temperature on either surface. Metal provides high strength along with elasticity, and ceramic provide thermal insulation to the FGM.

Many analysts have committed to the response of functionally graded (FG) plates by applying either 3D theories or ESL theories. Vel and Batra [1] developed a three-dimensional (3D) mathematical solution to capture a simply supported FG plate's static deformation. The study was carried out for transient thermal load. Further, the classical plate theory (CPT), which avoids normal and shear deformation, applicable for a thin plate, was introduced. Using this method, Javaheri and Eslami [2] calculate the FG plate's buckling load for uniform, linear/nonlinear temperature variation. The application of the finite strip method along with CPT for buckling load calculation has been considered by Ghannadpour et al. [3]. For overcoming the potholes of CPT, first-order shear deformation theory (FOST) has invented. Damanpack et al. [4] assume straight-line variation of in-plane displacements in the depth direction; here, shear correction factors need to use. Shen [5] used FOST and a mixed Galerkin perturbation technique for calculating the nonlinear bending behavior of the FG plate. This FG Plate was subject to uniform and sinusoidal thermal load. Lanhe [6] carried out buckling load calculations under a stable temperature environment. With the help of the element-free Galerkin methodology and FOST, Dai et al. [7] study the FG plate's dynamic response with piezoelectric sensors and actuators. Nguyen [8] developed a FOST model to decide the shear correction factors for FG and sandwich FG plates.

To eliminate the need for shear correction factors, higher-order shear and normal deformation theories (HOSNT) have generated, considering the expansion of displacement components in power series. Yang and Shen [9] studied the nonlinear flexural response of the FG plate with higher-order shear deformation under constant temperature rise. Here elasticity constant, passion's ratio and thermal expansion coefficient assume to change as per power law. Zenkour [10] used generalized shear deformation theory to study FG plate HOST's bending behavior and formulated equilibrium and stability equations. This formulation was further decoupled by Saidi and Jomehzadeh [11]. Kadoli et al. [12] used HOST to study the effect of loading position on the ceramic and metal face of the FG laminate. Mantri et al. [13] presented a new HOST for the bending response of the FG plate. Kant et al. [14] used HOSNT associated with eleven degrees of freedoms (DOFs) for stress analysis and free vibration of the FG plate.

Cubic variation of shear deformation theory has been developed for considering transverse shear deformation impacts and for fulfillments of zero traction boundary conditions. Using this theory, Ferreria et al. [15] obtained the static analysis results, which has correlated with the Meshless

method's outcomes. Akbarzadeh et al. [16], with TSDT, achieved an FG plate response for uniform mechanical and dynamic loading. Wu and Li [17] obtained a reaction of the FG plate for sinusoidal loading. Further, Xing et al. [18] worked on the same area with the n^{th} order theory. All these researchers considered material variation as per power-law.

Research of Functionally graded plates in sandwich form has been conducted by many researchers. The base footing performs a major role in structural stability. The static behavior of advanced FG ceramic-metal plates supported on a flexible foundation and exposed to hygro-thermo-mechanical loading has been documented by Tounsi et al. [19]. Chikr et al. [20] presented modified shear deformation theory in trigonometric form and analyzed the FG sandwich plate supported by a flexible footing base with various parameters and support conditions. Later on, Refrafi [21] emphasized on buckling behavior of FG sandwich plate resting on flexible footing subjected to moisture, thermal and mechanical loading. Boussoula et al. [22] have applied shear deformation theory to examine FG sandwich plates' thermomechanical bending behavior by assuming E-FGM, P-FGM and S-FGM. Many examiners have also studied the dynamic behavior of FG materials. FG nano-plate with simple support has been analyzed for free vibration with nonlocal integral refined plate theory by Balubaid et al. [23]. Static and free vibration analyses for functionally graded pours sandwich plate on a flexible footing by a quasi-3D hyperbolic shear deformation formulation have been carried out by Kaddari et al. [24]. Here, along with other parameters porosity effect has been primarily discussed.

Interface study has another approach to study smart materials. Delamination, stress concentration, the requirement of smooth variation of temperature can be achieved with this approach below the melting point at the interfaces. Roy [25] used a multiphase PF approach to study barrierless nucleation for nitramine octahydro1,3,5,7-tetranitro 1,3,5,7-tetrazocine crystal. A similar approach of phase transition has also been studied by a group of few scientists, Henson et al. [26], Smibwitz et al. [27], Bowlan et al. [28] and Levitas et al. [29] etc.

Examine through past earlier documentation and realization of work done on FG materials uptilts and it has been observed that less literature is available for thermomechanical analysis of FG materials. Most researchers considered assumed thermal through thickness variation either constant, linearly varying, as per exponential, as per power law or as per sigmoid law. It has also been verified as very few studies have carried out with actual temperature distribution as per heat conduction law. Here, an attempt has been made to determine through thickness actual temperature profile by heat conduction law by developing novel semi-analytical formulation followed by stress analysis. This analysis is an extension of the semi-analytical formulation developed by Kulkarni and Pendhari [30] for FG 2D laminate. Here, simultaneously, bending stress analysis has been carried out for assumed power law variation (as most researchers considered), and it has compared with exact variation to verify the importance of the actual temperature profile.

The required elasticity and heat conduction formulations have considered here for the development of semi-analytical methods, includes illustrating two-point BVP governed by a group of coupled first-order ordinary differential equations (ODE's) (Equation 1) along with the thickness of a laminate on a basis from Kantorovich and Krylov [31] approach.

$$\frac{dy(z)}{dz} = D(z)\,y(z) + p(z) \tag{1}$$

Thermal loading has been determined as per the heat conduction equation and designed to access actual temperature variation. Further through the thickness, thermal change as per simple power law has considered. Material properties here are considered varied as per power law and Poisson's ratio has remained the same throughout the domain.

2. Mathematical formulations

A linearly flexible square/rectangular simply supported FG laminate of plan dimensions (a) and (b) and homogenous depth (h) is as indicated in Figure 1. It has been subjected to arbitrarily distributed thermo-mechanical loading at the upper surface and the downward surface is held traction-free and appearing as the reference temperature. The coefficient of thermal expansion (α), Elastic modulus (E), and coefficient of thermal conductivity (λ) have varied only through the thickness of laminate accordingly to a power law as,

$$\begin{aligned} E(z) &= E_b + \left[(E_t - E_b)\left(\frac{z}{h}\right)^k \right] \\ \lambda(z) &= \lambda_b + \left[(\lambda_t - \lambda_b)\left(\frac{z}{h}\right)^k \right] \\ \alpha(z) &= \alpha_b + \left[(\alpha_t - \alpha_b)\left(\frac{z}{h}\right)^k \right] \end{aligned} \tag{2}$$

Where, E_b and E_t be Young's elasticity constants, α_b and α_t be constant of thermal expansion, λ_b and λ_t are the coefficient of thermal conductivity at the lower and upper face of the laminate, respectively.

Next, it has been assumed that the FG material is homogenous and the ratio of lateral strain versus linear strain is assumed to be constant throughout the thickness.

3. Semi-analytical formulation for 3-dimensional heat conduction

FG materials are mainly used in the environment where structures are experiencing large temperatures. Hence, accurate determination of structural responses is of the utmost importance. This section is devoted to the discussion of the closed-form formulation for the 3D heat conduction equation. A thermal load and heat flux as defined in Eqn. (3) is assumed with only known temperature values at the top and bottom of the laminate surface $(T = T_b \text{ at } z = 0 \text{ and } T = T_t \text{ at } z = h)$.

$$T(x,z) = \sum_{m=1}^{\infty} T(z)\sin\frac{m\pi x}{a}\sin\frac{n\pi y}{b} \qquad q_z(x,z) = \sum_{m=1}^{\infty} q_z(z)\sin\frac{m\pi x}{a}\sin\frac{n\pi y}{b} \tag{3}$$

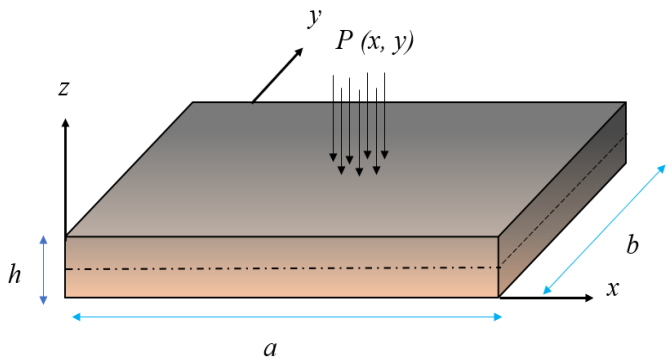

Fig. 1. FG 3D laminate exposed to thermal loading.

A governing two-dimensional (3D) steady-state heat conduction equation without internal heat generation is,

$$\lambda(z)\frac{\partial^2 T(x,z)}{\partial x^2}+(z)\frac{\partial^2 T(x,z)}{\partial y^2}+\lambda(z)\frac{\partial^2 T(x,z)}{\partial z^2}=0 \tag{4}$$

As per heat conduction law given by Fourier, heat flux in *x, y* and *z* directions are as below

$$q_x(x,z)=-\lambda(z)\frac{\partial T(x,z)}{\partial x}\ ,\ q_y(x,z)=-\lambda(z)\frac{\partial T(x,z)}{\partial y}\ ,\ q_z(x,z)=-\lambda(z)\frac{\partial T(x,z)}{\partial z} \tag{5}$$

where, q_i = heat flux along *x*, y and *z*-axis (i = *x*, y, *z*) in Wm^{-2}

And, with the consideration, the heat flow maintains the amount of total heat in element zero, the equilibrium equation in 3D,

$$\frac{\partial q_x(x,z)}{\partial x}+\frac{\partial q_y(x,z)}{\partial y}+\frac{\partial q_z(x,z)}{\partial z}=0 \tag{6}$$

Two variables, viz. temperature field (T) and heat flux (q_z) are assumed as the primary variable. With the help of algebraic simplification of the Eqns. (5) and (6) a set of PDEs consisting of only two primary variables q_z and T are obtained.

$$\frac{\partial T(x,z)}{\partial z}=-\frac{1}{\lambda(z)}q_z(x,z) \qquad \frac{\partial q_z(x,z)}{\partial z}=\lambda(z)\frac{\partial^2 T(x,z)}{\partial x^2}+\lambda(z)\frac{\partial^2 T(x,z)}{\partial y^2} \tag{7}$$

Substituting Eqn. (3) and its differential coefficients into Eqn. (7). The set of the first-order ODEs obtained as,

$$\frac{dT(z)}{dz}=-\frac{1}{\lambda}q_z(z) \qquad \frac{dq_z(z)}{dz}=-\lambda(z)\left(\frac{m^2\pi^2}{a^2}+\frac{n^2\pi^2}{b^2}\right)T(z) \tag{8}$$

An equation has given the governing two-point BVP in ODEs in the field with the known temperature at the upper and lower FG laminate surface. (8).

4. The semi-analytical formulation for 3-dimensional stress analysis

As per the basic linear theory of elasticity, three-dimensional (3D) strain-displacement relationship, equilibrium equations, and constitutive relations in the thermo-elastic environment can be given as,

$$\varepsilon_x = \frac{\partial u}{\partial x} \qquad \varepsilon_y = \frac{\partial v}{\partial y} \qquad \varepsilon_z = \frac{\partial w}{\partial z}$$
$$\gamma_{xz} = \frac{\partial u}{\partial z} + \frac{\partial w}{\partial x} \qquad \gamma_{yz} = \frac{\partial v}{\partial z} + \frac{\partial w}{\partial y} \qquad \gamma_{xy} = \frac{\partial u}{\partial y} + \frac{\partial v}{\partial x} \tag{9}$$

$$\frac{\partial \sigma_x}{\partial x} + \frac{\partial \tau_{xy}}{\partial y} + \frac{\partial \tau_{xz}}{\partial z} + B_x = 0$$
$$\frac{\partial \tau_{yx}}{\partial x} + \frac{\partial \sigma_y}{\partial y} + \frac{\partial \tau_{yz}}{\partial z} + B_y = 0 \tag{10}$$
$$\frac{\partial \tau_{zx}}{\partial x} + \frac{\partial \tau_{zy}}{\partial y} + \frac{\partial \sigma_z}{\partial z} + B_z = 0$$

$$\begin{Bmatrix} \sigma_x \\ \sigma_y \\ \sigma_z \\ \tau_{xy} \\ \tau_{xz} \\ \tau_{yz} \end{Bmatrix} = \begin{bmatrix} C_{11} & C_{12} & C_{13} & 0 & 0 & 0 \\ & C_{22} & C_{23} & 0 & 0 & 0 \\ & & C_{33} & 0 & 0 & 0 \\ & & & C_{44} & 0 & 0 \\ & \textit{symmetric} & & & C_{55} & 0 \\ & & & & & C_{66} \end{bmatrix} \begin{Bmatrix} \varepsilon_x - \alpha_x T \\ \varepsilon_y - \alpha_y T \\ \varepsilon_z - \alpha_z T \\ \gamma_{xy} \\ \gamma_{xz} \\ \gamma_{yz} \end{Bmatrix} \tag{11}$$

Here $\alpha_x T, \alpha_y T$ and $\alpha_z T$ are the thermal expansions generated due to thermal change without constraints and B_x, B_y, B_z are the forces acting per unit volume in *x, y* and *z*-direction, respectively generally called body forces, which has ignored in the numerical examination for the sake of simplicity. Material coefficients C_{ij} are elastic constants, and for the FG material a constitutive relation can be given as,

$$C_{11} = C_{22} = C_{33} = \frac{E(z)(1-\upsilon^2)}{(1-3\upsilon^2-2\upsilon^3)} \qquad C_{12} = C_{13} = C_{23} = \frac{E(z)(\upsilon+\upsilon^2)}{(1-3\upsilon^2-2\upsilon^3)} \qquad C_{44} = C_{55} = C_{66} = \frac{E(z)}{2(1+\upsilon)} \tag{12}$$

The above Eqns. (9), (10) and (11) contain eight unknowns in eight equations which have as $u, v, w, \varepsilon_x, \varepsilon_y, \varepsilon_z, \sigma_x, \sigma_y, \sigma_z, \gamma_{xy}, \gamma_{xz}, \gamma_{yz}, \tau_{xy}, \tau_{xz}$ *and* τ_{yz}. After a simple algebraic reduction/manipulation of the basic elasticity equations, a set of PDEs includes only six dependent variables u, v, w, σ_z, τ_{xz} and τ_{yz} gained as below,

$$\frac{\partial u}{\partial z} = -\frac{\partial w}{\partial x} + \left(\frac{C_{66}}{C_{55}C_{66}} \right) \tau_{xz},$$

$$\frac{\partial v}{\partial z} = -\frac{\partial w}{\partial y} + \left(\frac{C_{55}}{C_{55}C_{66}} \right) \tau_{yz}$$

$$\frac{\partial w}{\partial z} = \frac{\sigma_z}{C_{33}} - \frac{1}{C_{33}} \left(C_{31} \frac{\partial u}{\partial x} + C_{32} \frac{\partial v}{\partial y} \right) + \frac{\alpha T}{C_{33}} \left(C_{31} + C_{32} + C_{33} \right)$$

$$\frac{\partial \tau_{xz}}{\partial z} = -\left(C_{11} - \frac{C_{13}C_{31}}{C_{33}} \right) \frac{\partial^2 u}{\partial x^2} - C_{44} \frac{\partial^2 u}{\partial y^2} - \left(C_{12} + C_{44} - \frac{C_{13}C_{32}}{C_{33}} \right) \frac{\partial^2 v}{\partial x \partial y}$$

$$- \frac{C_{13}}{C_{33}} \frac{\partial \sigma_z}{\partial x} + \begin{bmatrix} \left(C_{11} + C_{12} + C_{13} \right) \\ - \frac{C_{13}}{C_{33}} \left(C_{31} + C_{32} + C_{33} \right) \alpha . \frac{\partial T}{\partial x} \end{bmatrix} \tag{13}$$

$$\frac{\partial \tau_{yz}}{\partial z} = -\left(C_{21} + C_{44} - \frac{C_{23}C_{31}}{C_{33}} \right) \frac{\partial^2 u}{\partial x \partial y} - C_{44} \frac{\partial^2 v}{\partial x^2} - \left(C_{22} - \frac{C_{23}C_{32}}{C_{33}} \right) \frac{\partial^2 v}{\partial y^2}$$

$$- \frac{C_{23}}{C_{33}} \frac{\partial \sigma_z}{\partial y} + \begin{bmatrix} \left(C_{11} + C_{12} + C_{13} \right) \\ - \frac{C_{23}}{C_{33}} \left(C_{31} + C_{32} + C_{33} \right) \alpha . \frac{\partial T}{\partial y} \end{bmatrix}$$

$$\frac{\partial \sigma_z}{\partial z} = -\frac{\partial \tau_{xz}}{\partial x} - \frac{\partial \tau_{yz}}{\partial y}$$

With the help of boundary conditions at the support $x = 0$ and a and Fourier trigonometric series expansion, the PDE's given in equation (13) can convert into coupled first-order ODE as,

$$u(x, y, z) = \sum_{mn} u_{mn}(z) \cos \frac{m\pi x}{a} \sin \frac{n\pi y}{b}$$

$$v(x, y, z) = \sum_{mn} v_{mn}(z) \sin \frac{m\pi x}{a} \cos \frac{n\pi y}{b} \tag{14}$$

$$w(x, y, z) = \sum_{mn} w_{mn}(z) \sin \frac{m\pi x}{a} \sin \frac{n\pi y}{b}$$

and from the fundamental relations of the theory of elasticity, it can be shown that,

$$\tau_{xz}(x, y, z) = \sum_{mn} \tau_{xzmn}(z) \sin \frac{n\pi y}{b} \cos \frac{m\pi x}{a}$$

$$\tau_{yz}(x, y, z) = \sum_{mn} \tau_{yzmn}(z) \sin \frac{m\pi x}{a} \cos \frac{n\pi y}{b} \tag{15}$$

$$\sigma_z(x, y, z) = \sum_{mn} \sigma_{zmn}(z) \sin \frac{m\pi x}{a} \sin \frac{n\pi y}{b}$$

Further, applied transverse loading on the top of the FG laminate and temperature change along the *x*-direction is also given in the sinusoidal form as

$$p(x,y,z)=\sum_{m,n}^{\infty} p_{mn}\sin\frac{m\pi x}{a}\sin\frac{m\pi y}{b}$$
$$T(x,y,z)=\sum_{m,n}^{\infty} T(z)\sin\frac{m\pi x}{a}\sin\frac{m\pi y}{b} \tag{16}$$

Putting Eqns. (14), (15) and (16) and it is differential coefficients into Eqn. (13) Ordinary differential equations (ODEs), as mentioned in equation (17), have been received.

$$\begin{aligned}
\frac{du_{mn}(z)}{dz}&=\left(-\frac{m\pi}{a}\right)w_{mn}(z)+\left(\frac{1}{C_{55}}\right)\tau_{xzmn}(z)\\
\frac{dv_{mn}(z)}{dz}&=\left(-\frac{n\pi}{b}\right)w_{mn}(z)+\left(\frac{1}{C_{66}}\right)\tau_{yzmn}(z)\\
\frac{dw_{mn}(z)}{dz}&=\left(\frac{C_{31}}{C_{33}}\frac{m\pi}{a}\right)u_{mn}(z)+\left(\frac{C_{32}}{C_{33}}\frac{n\pi}{b}\right)v_{mn}(z)\\
&\quad+\left(\frac{1}{C_{33}}\right)\sigma_{zm}(z)+\alpha\left(\begin{matrix}C_{13}+C_{23}\\+C_{33}\end{matrix}\right)T(z)\\
\frac{d\tau_{xzmn}(z)}{dz}&=\left(C_{11}-\frac{C_{13}C_{31}}{C_{33}}\right)\left(\frac{m^2\pi^2}{a^2}\right)u_{mn}(z)+\left(C_{44}\frac{n^2\pi^2}{b^2}\right)u_{mn}(z)+\left(C_{12}+C_{44}-\frac{C_{13}C_{32}}{C_{33}}\right)\left(\frac{mn\pi^2}{ab}\right)v_{mn}(z)\\
&\quad-\left(\frac{C_{13}}{C_{33}}\frac{m\pi}{a}\right)\sigma_{zm}(z)+\left[\left(C_{11}+C_{12}+C_{13}\right)-\frac{C_{13}}{C_{33}}\left(C_{13}+C_{23}+C_{33}\right)\right]\left(\frac{m\pi}{a}\right)\alpha T(z)\\
\frac{d\tau_{yzmn}(z)}{dz}&=\left(C_{21}+C_{44}-\frac{C_{23}C_{31}}{C_{33}}\right)\left(\frac{mn\pi^2}{ab}\right)u_{mn}(z)+\left(C_{44}\frac{m^2\pi^2}{a^2}\right)v_{mn}(z)\\
&\quad+\left(C_{22}-\frac{C_{23}C_{32}}{C_{33}}\right)\left(\frac{n^2\pi^2}{b^2}\right)v_{mn}(z)-\left(\frac{C_{23}}{C_{33}}\frac{n\pi}{b}\right)\sigma_{zm}(z\\
&\quad+\left[\left(C_{12}+C_{22}+C_{23}\right)-\frac{C_{23}}{C_{33}}\left(C_{13}+C_{23}+C_{33}\right)\right]\left(\frac{n\pi}{b}\right)\alpha T(z)\\
\frac{d\sigma_{zm}(z)}{dz}&=\left(\frac{m\pi}{a}\right)\tau_{xzm}(z)+\left(\frac{n\pi}{b}\right)\tau_{yzm}(z)
\end{aligned} \tag{17}$$

Eqn. (17) represents the governing two-point BVP in ODEs in the domain $0\le z\le h$ with stress components known at the top and bottom surfaces of an FG laminate.

In the absence of a boundary layer effect, the numerical integration of the BVP has been defined in Eqns. (8), (17), and the related peripherical conditions can transform into a set of IVP's one non-homogeneous and $n/2$ homogeneous, equal to 2 and 4 for heat conduction and stress analysis formulation, respectively. BVP transformation to IVP for thermal and stress analysis has tabulated in Tables 1 and 2 successively. After this formation of a linear mixture of one non-homogeneous and $n/2$ homogeneous solution, fulfilling boundary conditions $z=h$ have been solved. These give rise to $n/2$ linear algebraic equations, which determine the unknown $n/2$ components at the starting edge $z=0$. Then a final numerical integration of Eqns. (8) (16)

represents the required outputs. The fourth-order Runge-Kutta technique has been applied here for numerical integration.

Table 1
Transformation of BVP into IVP's for thermal analysis

Integration No.	Bottom edge ($z = 0$)		Top edge ($z =$?)	
	$T(z)$	$q_z(z)$	$T(z)$	$q_z(z)$
1	Known	0 (Assumed)	M_{11}	M_{21}
2	0 (Assumed)	1 (Assumed)	M_{12}	M_{22}
3 (Final)	$T(0)$ (known)	$K1$	T(?) (known)	q_z(?)

Table 2. Transformation of BVP into IVP's for stress analysis

Integration No.	Bottom edge $(z = 0)$						Top edge $(z = h)$						Load term
	u	v	w	τ_{xz}	τ_{yz}	σ_z	u	v	w	τ_{xz}	τ_{yz}	σ_z	
1	0 (assumed)	0 (assumed)	0 (assumed)	0 (known)	0 (known)	0 (known)	Y_{11}	Y_{21}	Y_{31}	Y_{41}	Y_{51}	Y_{61}	Include
2	1 (assumed)	0 (assumed)	0 (assumed)	0 (assumed)	0 (assumed)	0 (assumed)	Y_{12}	Y_{22}	Y_{32}	Y_{42}	Y_{52}	Y_{62}	Delete
3	0 (assumed)	1 (assumed)	0 (assumed)	0 (assumed)	0 (assumed)	0 (assumed)	Y_{13}	Y_{23}	Y_{33}	Y_{43}	Y_{53}	Y_{63}	Delete
4	0 (assumed)	0 (assumed)	1 (assumed)	0 (assumed)	0 (assumed)	0 (assumed)	Y_{14}	Y_{24}	Y_{34}	Y_{44}	Y_{54}	Y_{64}	Delete
Final	X_1	X_2	X_3	0 (Known)	0 (Known)	0 (Known)	$u(h)$	$v(h)$	$w(h)$	0 (known)	0 (known)	0 (known)	Include

5. Numerical studies

Determination of exact thermal spreading through the depth of FG laminate and perform thermal stress analysis with present formulation; a computer code has developed. For validating generated computer code, stress analysis has been carried out for laminate subjected to mechanical loading with intensity $P_0 = 1.0\ MPa$ at the laminate's top. Obtained outputs have compared with Zenkour (2006) third-order shear deformation theory and Mantri's (2012) higher-order shear deformation theory, which has tabulated in Table 3 and close agreement between values has been observed. For the numerical study, reference temperature at the lower and upper surface of the FG plate has been considered $20^0 C$ and $300^0 C$ respected. As listed in table 4, three material sets have supposed to examine the effect of material gradation on temperature distribution. Various power indices (k) have considered from ceramic to metal variation of material gradation within thickness. Based on convergence studies, around 20 to 30 steps have been used through the thickness of laminate for numerical integration. Distribution of actual

temperature compared with assumed temperature as per power law variation through FG plate depth with equal dimension for all material sets (aspect ratios 5 to 50) has plotted in figures 2,3 and 4. Moreover, to observe the effect of a different side to length ratio $\left(b/a\right)$, a comparison of actual and assumed temperature variation had depicted in figure 5 only for material set B.

From graphs 2,3,4 and 5, it has been seen that the exact temperature profile for all aspect ratios for a particular *k* index follows the same pattern, there has no or little variation observed from thin to thick plate consideration. For power index (*k*) is 0 and 1, the Model 2 assumed temperature profile overestimates the Model 1 actual temperature profile. For power index (*k*) 2 and 4, both this variation partially coincides with each other, and further for power index (*k*) 8 and 10 assumed temperature profile by Model 2 underestimate Model 1 actual temperature profile. This observation has valid for all material sets. It is worth to be noted that Model 2, through thickness temperature variation, remains almost constant for power index, *k*=0, and for power index, *k*=1, it turns to be perfectly linear.

Further, it has taken the higher-order curve's shape as the power index increases (*k*=1,4,8 and 10). However, Model 2, through thickness temperature distribution, was noted to be linear for power index *k*=0 and further changes to higher-order curve for power index, *k*=1, 2, and 4. However, for the power index, *k*=8, and 10, this variation is nearly linear again. Again, these observations have valid for all material properties and in-plane aspect ratios (*b/a*).

Determination of through thickness thermal stress variation for exact (Model 1) and with assumed power law (Model 2) temperature profile, a computer code has developed. For comparison of obtained results following normalization coefficient have used,

$$\bar{u}=\frac{100u}{\alpha_b T_b s^3};\ \bar{v}=\frac{100v}{\alpha_b T_b s^3};\ \bar{w}=\frac{10w}{\alpha_b T_b s^4};\ \ \bar{\sigma}_x=\frac{20\sigma_x}{E_b\alpha_b T_b s^2};\bar{\sigma}_y=\frac{20\sigma_y}{E_b\alpha_b T_b s^2};$$
$$\bar{\tau}_{xy}=\frac{20\tau_{xy}}{E_b\alpha_b T_b s^2};\ \bar{\tau}_{xz}=\frac{100\tau_{xz}}{E_b\alpha_b T_b s};\bar{\tau}_{yz}=\frac{100\tau_{yz}}{E_b\alpha_b T_b s} \tag{18}$$

Obtained results have been tabulated in tables 5, 6, and 7 for square plate material sets A, B, and C, respectively, simultaneously for rectangular plates in tables 8, 9, and 10. Table 5 noted that the average percentage difference between Model 2 and Model 1 for in plane displacement $\left(\bar{u}\right)$ is 30% for transverse movement $\left(\bar{w}\right)$ 46%, for in normal plane stress $\left(\bar{\sigma}_x\right)$ 66%, for in plane shear stress $\left(\bar{\tau}_{xy}\right)$ is 30% and for transverse shear stress $\left(\bar{\tau}_{xz}\right)$is 53%. Further from table 5 and table 6, it has been observed that these percentage variations outcomes decrease for material group B and increases for material group C.

By observing values in tables 8, 9 and 10, some observations have been documented. Average percentage variation between Model 2 and Model 1 results in plane displacements $\left(\bar{u},\bar{v}\right)$, in the plane, direct stress in the y-direction ($\bar{\sigma}_y$), and for in plane shear stress has ($\bar{\tau}_{xy}$) not more. For

in plane normal stress in the x-direction ($\bar{\sigma}_x$)and transverse shear stress ($\bar{\tau}_{xz}, \bar{\tau}_{yz}$) shows variations in values; similarly, it has also been observed that transverse displacement $(\bar{w})$ remains silent. These have valid for all material sets considered for the study.

Through thickness variation of thermal stress analyses for Model 1 and Model 2 have depicted in figure 6 to 10 for in plane displacement $(\bar{u})$, transverse displacement $(\bar{w})$, in the plane, direct stress $(\bar{\sigma}_x)$, in the plane, and transverse shear stresses $(\bar{\tau}_{xy}, \bar{\tau}_{xz})$, respectively. Plate with material set B with equal dimension has only been considered for demonstration of results in Figure.

From figure (6 to 10), It is worth noting that there is a significant difference in thermal stress analyses performed for actual and assumed temperature variation along with the depth of the plate. The notable differences in numerical results are less for moderately thick plates $(s=10)$ than reasonably thin and thin plates. Also, material dependency has been observed in numerical results. In the present analysis, material set B is more sensitive than material sets A and C for all displacement and stresses parameters. There is the impact of power index (k) on numerical values. More overestimation underestimation has been noted for power index (k) represented ceramic class of material almost for all displacement and stress variables. However, more or less, the same pattern of variations has been observed in all figures for Model 1 and Model 2 analyses except for transverse shear stress $(\bar{\tau}_{xz})$, which has been depicted in figure 10, showing exact opposite stress patterns. The laminate's thickness has a governing parameter for stress analysis; a thick laminate is more susceptible to temperature changes. Hence shows more error in Model 1 and Model 2 outputs than the moderately thick and thin laminates.

Table 3

Normalized in-plane and transverse displacements $[\bar{u}, \bar{w}]$, in-plane normal and shear stresses $[\bar{\sigma}_{xx}, \bar{\tau}_{xy}]$ and transverse shear stresses $_{[\bar{\tau}_{xz}]}$ of square FG laminate under bi-directional transverse sinusoidal loading for side to thickness ratio 10 for Mechanical Loading for material set B.

Quantity	Theories	k					
		0	**1**	**2**	**4**	**8**	**10**
$\bar{u}\left(-\frac{h}{4}\right)$	Model 1	0.2198	0.6436	0.9012	1.0541	1.0820	1.0840
	Zenkour [2006][a]	0.2309	0.6626	0.9281	1.0941	1.1340	1.1372
	Mantari et al. [2012][b]	-	0.6398	0.8957	1.0457	1.0709	-
$\bar{w}(0)$	Model 1	0.2940	0.5870	0.757	0.8822	0.97Z	1.0070
	Zenkour [2006][a]	0.2960	0.5889	0.7573	0.8819	0.975	1.0089
	Mantari et al. [2012][b]	-	0.5880	0.7564	0.8814	0.9737	-
$\bar{\sigma}_x\left(\frac{h}{3}\right)$	Model 1	2.0043	3.097	3.6247	4.0838	4.7555	5.0660
	Zenkour [2006][a]	1.9955	1.4894	1.3954	1.1783	0.9466	5.0890
$\bar{\tau}_{xy}\left(-\frac{h}{3}\right)$	Model 1	0.6826	0.6830	0.5115	0.5623	0.5840	0.6016
	Zenkour [2006][a]	0.7065	0.6110	0.5441	0.5667	0.5856	0.5894
	Mantari et al. [2012][b]	-	0.6112	0.5438	0.5662	0.5850	-
$\bar{\tau}_{xz}\left(\frac{h}{6}\right)$	Model 1	0.2383	0.2382	0.2256	0.2175	0.2166	0.2166
	Zenkour [2006][a]	0.2462	0.2622	0.2763	0.2580	0.2121	0.2198
	Mantari et al. [2012][b]	-	0.2566	0.2741	0.2623	0.2140	-

Note: Zenkour [2006][a] =Generalized TSDT and Mantari et al. [2012][b] = HSDT

Table 4. Material Properties

Set	Material Properties
A	At bottom, $z = 0 \Rightarrow$ Aluminium: $E = 70\ GPa$ $\mu = 0.3$ λ=204 K^{-1} $\alpha = 23 \times 10^{-6}\ W_m^{-1}K^{-1}$ At top, $z = h \Rightarrow$ Zirconia : $E = 151\ GPa$ $\mu = 0.3$ λ=2.09 K^{-1} $\alpha = 10 \times 10^{-6}\ W_m^{-1}K^{-1}$
B	At bottom, $z = 0 \Rightarrow$ Aluminium: $E = 70\ GPa$ $\mu = 0.3$ λ=204K^{-1} $\alpha = 23 \times 10^{-6}\ W_m^{-1}K^{-1}$ At top, $z = h \Rightarrow$ Alumina : $E = 380\ GPa$ $\mu = 0.3$ $\lambda = 10.40K^{-1}$ $\alpha = 7.4 \times 10^{-6}\ W_m^{-1}K^{-1}$
C	At bottom, $z = 0 \Rightarrow$ Monel : $E = 227.24\ GPa$ $\mu = 0.3$ λ=25 K^{-1} $\alpha = 15 \times 10^{-6}\ W_m^{-1}K^{-1}$ At top, $z = h \Rightarrow$ Zirconia : $E = 151\ GPa$ $\mu = 0.3$ λ=2.09 K^{-1} $\alpha = 10 \times 10^{-6}\ W_m^{-1}K^{-1}$

Ref. Kadoli et al. [12]

Table 5. Normalized in plane and transverse displacements $(\bar{u}, \bar{w})$ and stresses $\left(\bar{\sigma}_{xx}, \bar{\tau}_{xy}, \bar{\tau}_{xz}\right)$ of square FG plate under bi-direction sinusoidal transverse loading for side to thickness ratio 5.0 and 10.0 for material set A

s	*k*	Model	$\bar{u}\left(a, 0, 0\ \&\ h\right)$		$\bar{w}\left(a/2, b/2 \max\right)$	$\bar{\sigma}_{xx}\left(a/2, 0, 0\ \&\ h\right)$		$\bar{\tau}_{xy}\left(a/2, 0, 0\ \&\ h\right)$		$\bar{\tau}_{xz}\left(0, 0, \max\right)$
5	0	Model 1	-5.491	-0.660	0.149	-5.447	-00.555	-5.724	-0.319	0.411
		Model 2	-5.483	-7.407	-0.060	-5.461	-10.568	-5.717	-3.580	1.293
	1	Model 1	-3.414	-0.476	0.092	-9.468	-0.715	-3.559	-0.230	1.473
		Model 2	-6.591	-2.374	0.128	-3.317	0.988	-6.872	-1.148	4.590
	2	Model 1	-3.721	-0.822	0.125	-8.874	-0.405	-3.879	-0.397	0.610
		Model 2	-6.349	-0.522	0.238	-3.786	-0.674	-6.619	-0.252	2.135
	4	Model 1	-4.316	-1.069	0.100	-7.722	-0.183	-4.499	-0.517	1.022
		Model 2	-5.428	0.354	0.179	-5.569	-1.460	-5.659	0.171	2.947
	8	Model 1	-5.088	-1.111	0.172	-6.226	-0.145	-5.305	-0.537	1.533
		Model 2	-4.205	0.363	0.175	-7.937	-1.469	-4.384	0.176	3.742
	10	Model 1	-5.341	-1.085	0.183	-5.737	-0.169	-5.568	-0.524	1.490
		Model 2	-3.824	0.278	0.157	-8.673	-1.392	-3.987	0.134	3.610
10	0	Model 1	-1.372	-0.168	0.038	-1.364	-0.136	-1.430	-0.081	0.411
		Model 2	-1.303	-1.772	-0.015	-1.497	-2.714	-1.358	-0.856	0.507
	1	Model 1	-0.863	-0.117	0.024	-2.349	-0.180	-0.900	-0.057	1.473
		Model 2	-1.601	-0.544	0.024	-0.919	0.203	-1.670	-0.263	0.986
	2	Model 1	-0.952	-0.213	0.026	-2.176	-0.094	-0.993	-0.103	0.610
		Model 2	-1.549	-0.093	0.050	-1.021	-0.202	-1.615	-0.045	0.424
	4	Model 1	-1.122	-0.283	0.026	-1.847	-0.031	-1.170	-0.137	1.022
		Model 2	-1.326	0.117	0.046	-1.453	-0.391	-1.382	0.056	0.816
	8	Model 1	-1.341	-0.296	0.036	-1.423	-0.020	-1.398	-0.143	1.533
		Model 2	-1.026	0.113	0.038	-2.034	-0.387	-1.069	0.054	0.997
	10	Model 1	-1.412	-0.289	0.039	-1.286	-0.026	-1.472	-0.140	1.490
		Model 2	-0.932	0.090	0.034	-2.215	-0.366	-0.972	0.043	0.960

Table 6. Normalized in plane and transverse displacements $(\bar{u},\bar{w})$ and stresses $\left(\bar{\sigma}_{xx},\bar{\tau}_{xy},\bar{\tau}_{xz}\right)$ of square FG plate under bi-direction sinusoidal transverse loading for side to thickness ratio 5.0 and 10.0 for material set B

s	k	Model	$\bar{u}\left(a,0,0\ \&\ h\right)$		$\bar{w}\left(a/2,b/2\ \max\right)$	$\bar{\sigma}_{xx}\left(a/2,0,0\ \&\ h\right)$		$\bar{\tau}_{xy}\left(a/2,0,0\ \&\ h\right)$		$\bar{\tau}_{xz}\left(0,0,\max\right)$
5	0	Model 1	-4.168	-0.637	0.109	-09.867	-00.593	-10.722	-0.302	1.265
		Model 2	-4.040	-6.259	-0.069	-10.518	-11.970	-10.391	-2.966	3.424
	1	Model 1	-3.604	-0.832	0.086	-12.721	-0.412	-09.272	-0.394	0.780
		Model 2	-5.244	-3.010	0.065	-04.423	1.619	-13.489	-1.426	10.574
	2	Model 1	-4.110	-1.413	0.082	-10.161	0.130	-10.573	-0.670	2.604
		Model 2	-5.364	-1.074	0.127	-03.816	-0.186	-13.798	-0.509	7.482
	4	Model 1	-5.071	-1.872	0.093	-5.298	0.558	-13.045	-0.887	6.294
		Model 2	-4.938	0.141	0.157	-5.971	-1.318	-12.703	0.067	2.380
	8	Model 1	-0.048	0.003	0.128	-0.066	-0.015	-00.124	0.001	0.029
		Model 2	-6.374	-1.993	0.146	1.296	0.671	-16.396	-0.944	8.669
	10	Model 1	-0.041	0.005	0.142	-0.103	-0.017	-00.105	0.002	0.043
		Model 2	-6.818	-1.967	0.138	3.543	0.646	-17.539	-0.932	8.652
10	0	Model 1	-1.041	-0.163	0.030	-2.473	-0.145	-02.678	-0.077	0.318
		Model 2	-0.957	-1.497	0.000	-2.897	-3.055	-02.462	-0.709	1.291
	1	Model 1	-0.906	-0.211	0.022	-3.158	-0.100	-02.329	-0.100	0.192
		Model 2	-0.906	-0.211	0.018	-1.282	0.355	-03.283	-0.331	2.356
	2	Model 1	-1.041	-0.371	0.021	-2.472	0.049	-02.678	-0.176	0.732
		Model 2	-1.313	-0.226	0.034	-1.094	-0.086	-03.379	-0.107	1.686
	4	Model 1	-1.296	-0.496	0.025	-1.180	0.166	-03.335	-0.235	1.739
		Model 2	-1.212	0.067	0.040	-1.607	-0.359	-03.118	0.032	0.691
	8	Model 1	-4.181	0.375	0.035	-9.803	-1.536	-10.755	0.178	3.971
		Model 2	-1.635	-0.525	0.037	0.536	0.193	-04.207	-0.249	2.355
	10	Model 1	-3.926	0.338	0.038	-11.096	-1.502	-10.098	0.160	3.993
		Model 2	-1.749	-0.517	0.034	01.113	0.185	-04.500	-0.245	2.343

Table 7. Normalized in plane and transverse displacements $(\bar{u}, \bar{w})$ and stresses $\left(\bar{\sigma}_{xx}, \bar{\tau}_{xy}, \bar{\tau}_{xz}\right)$ of square FG plate under bi-direction sinusoidal transverse loading for side to thickness ratio 5.0 and 10.0 for material set C

s	k	Model	$\bar{u}\left(a, 0, 0 \& h\right)$		$\bar{w}\left(a/2, b/2 \max\right)$	$\bar{\sigma}_{xx}\left(a/2, 0, 0 \& h\right)$		$\bar{\tau}_{xy}\left(a/2, 0, 0 \& h\right)$		$\bar{\tau}_{xz}\left(0, 0, \max\right)$
5	0	Model 1	-8.319	-0.725	0.234	-2.193	-0.492	-2.238	-0.352	0.067
		Model 2	-8.597	-9.857	-0.039	-2.055	-8.295	-2.312	-4.788	0.321
	1	Model 1	-6.467	-0.383	0.187	-3.114	-0.799	-1.740	-0.186	1.087
		Model 2	-9.402	-1.641	0.240	-1.655	0.330	-2.529	-0.797	1.452
	2	Model 1	-6.760	-0.669	0.188	-2.969	-0.542	-1.818	-0.325	0.535
		Model 2	-8.170	0.037	0.251	-2.268	-1.176	-2.197	0.018	1.340
	4	Model 1	-7.608	-0.917	0.206	-2.547	-0.320	-2.046	-0.445	0.291
		Model 2	-6.131	0.541	0.205	-3.281	-1.629	-1.649	0.263	3.426
	8	Model 1	-8.805	-1.024	0.239	-1.952	-0.224	-2.368	-0.497	0.913
		Model 2	-4.144	0.289	0.138	-4.269	-1.402	-1.115	0.140	3.434
	10	Model 1	-9.190	-1.027	0.251	-1.761	-0.221	-2.472	-0.499	1.043
		Model 2	-3.626	0.156	0.119	-4.526	-1.283	-0.975	0.076	3.158
	0	Model 1	-2.079	-0.183	0.060	-0.549	-0.122	-0.559	-0.089	0.017
		Model 2	-2.042	-2.365	-0.010	-0.567	-2.163	-0.549	-1.149	0.149
10	1	Model 1	-1.621	-0.090	0.048	-0.776	-0.205	-0.436	-0.044	0.284
		Model 2	-2.273	-0.365	0.060	-0.452	0.042	-0.611	-0.178	0.274
	2	Model 1	-1.709	-0.169	0.049	-0.733	-0.134	-0.460	-0.082	0.130
		Model 2	-1.978	0.043	0.064	-0.599	-0.324	-0.532	0.021	0.407
	4	Model 1	-1.940	-0.237	0.054	-0.618	-0.073	-0.522	-0.115	0.091
		Model 2	-1.481	0.161	0.052	-0.846	-0.430	-0.398	0.078	0.924
	8	Model 1	-2.253	-0.264	0.063	-0.462	-0.049	-0.606	-0.128	0.265
		Model 2	-0.997	0.091	0.034	-1.087	-0.368	-0.268	0.044	0.909
	10	Model 1	-2.351	-0.264	0.066	-0.414	-0.049	-0.632	-0.128	0.296
		Model 2	-0.871	0.056	0.029	-1.149	-0.336	-0.234	0.027	0.835

Table 8. Normalized in plane and transverse displacements $(\bar{u},\bar{v},\bar{w})$ and stresses $(\bar{\sigma}_{xx},\bar{\sigma}_{yy},\bar{\tau}_{xy},\bar{\tau}_{xz},\bar{\tau}_{yz})$ of Rectangular FG plate under bi-direction sinusoidal transverse loading for side to thickness ratio 5.0 for material set A

b/a	k	Model	$\bar{u}(a,0,0\ \&\ h)$		$\bar{v}(0,b,0\ \&\ h)$		$\bar{w}(a/2,b/2,\max)$	$\bar{\sigma}_{xx}(a/2,0,0\ \&\ h)$		$\bar{\sigma}_{yy}(0,b/2,0\ \&\ h)$		$\bar{\tau}_{xy}(a/2,b/2,0\ \&\ h)$		$\bar{\tau}_{xz}(a/2,b/2,\max)$	$\bar{\tau}_{yz}(a/2,b/2,\max)$
1.5	0	Model 1	-7.474	-0.498	-4.983	-0.332	0.217	-3.461	-0.231	-7.791	-0.519	-5.195	-0.346	0.000	0.000
		Model 2	-7.822	-7.822	-5.214	-5.214	0.000	-2.875	-2.875	-7.405	-7.405	-5.437	-5.437	1.120	0.747
	1	Model 1	-4.745	-0.656	-3.163	-0.437	0.129	-8.069	-0.630	-10.817	-0.806	-3.298	-0.211	1.485	0.990
		Model 2	-9.032	-3.187	-6.021	-2.125	0.180	-0.832	1.351	-6.063	0.495	-6.278	-1.027	4.355	2.904
	2	Model 1	-5.194	-1.153	-3.463	-0.769	0.126	-7.311	-0.240	-10.319	-0.550	-3.610	-0.372	0.607	0.404
		Model 2	-8.713	-0.646	-5.809	-0.431	0.249	-1.371	-0.637	-6.417	-0.811	-6.056	-0.208	1.975	1.317
	4	Model 1	-6.058	-1.511	-4.039	-1.008	0.141	-5.851	0.040	-9.361	-0.366	-4.211	-0.487	1.099	0.733
		Model 2	-7.452	0.547	-4.968	0.365	0.250	-3.500	-1.571	-7.816	-1.424	-5.179	0.176	3.062	2.042
	8	Model 1	-7.177	-1.573	-4.785	-1.049	0.173	-3.963	0.088	-8.120	-0.334	-4.988	-0.507	1.664	1.110
		Model 2	-5.770	0.548	-3.846	0.365	0.200	-6.339	-1.571	-9.681	-1.424	-4.010	0.176	3.832	2.555
	10	Model 1	-7.541	-1.536	-5.027	-1.024	0.186	-3.349	0.059	-7.717	-0.353	-5.242	-0.495	1.622	1.081
		Model 2	-5.246	0.426	-3.497	0.284	0.181	-7.222	-1.476	-10.261	-1.362	-3.646	0.137	3.694	2.463
3.0	0	Model 1	-0.010	-0.001	-0.003	0.000	0.000	-0.011	-0.001	-0.101	-0.007	-0.034	-0.002	0.000	0.000
		Model 2	-0.010	-0.010	-0.003	-0.003	0.000	-0.006	-0.006	-0.099	-0.099	-0.035	-0.035	0.087	0.029
	1	Model 1	-0.006	-0.001	-0.002	0.000	0.000	-0.066	-0.005	-0.123	-0.009	-0.021	-0.001	0.149	0.050
		Model 2	-0.012	-0.004	-0.004	-0.001	0.000	0.019	0.018	-0.089	0.000	-0.041	-0.007	0.421	0.140
	2	Model 1	-0.007	-0.002	-0.002	-0.001	0.000	-0.056	-0.001	-0.119	-0.007	-0.024	-0.002	0.060	0.020
		Model 2	-0.011	-0.001	-0.004	0.000	0.000	0.013	-0.006	-0.092	-0.009	-0.039	-0.001	0.188	0.063
	4	Model 1	-0.008	-0.002	-0.003	-0.001	0.000	-0.039	0.003	-0.112	-0.006	-0.028	-0.003	0.115	0.038
		Model 2	-0.010	0.001	-0.003	0.000	0.000	-0.012	-0.017	-0.102	-0.014	-0.033	0.001	0.313	0.104
	8	Model 1	-0.009	-0.002	-0.003	-0.001	0.000	-0.016	0.003	-0.103	-0.006	-0.033	-0.003	0.175	0.058
		Model 2	-0.007	0.001	-0.002	0.000	0.000	-0.046	-0.017	-0.115	-0.014	-0.026	0.001	0.389	0.130
	10	Model 1	-0.010	-0.002	-0.003	-0.001	0.000	-0.008	0.003	-0.100	-0.006	-0.034	-0.003	0.171	0.057
		Model 2	-0.007	0.001	-0.002	0.000	0.000	-0.056	-0.016	-0.119	-0.013	-0.024	0.001	0.374	0.125

Table 9. Normalized in plane and transverse displacements $(\bar{u},\bar{v},\bar{w})$ and stresses $(\bar{\sigma}_{xx},\bar{\sigma}_{yy},\bar{\tau}_{xy},\bar{\tau}_{xz},\bar{\tau}_{yz})$ of Rectangular FG plate under bi-direction sinusoidal transverse loading for side to thickness ratio 5.0 for material set B

b/a	k	Model	$\bar{u}(a,0,0\ \&\ h)$		$\bar{v}(0,b,0\ \&\ h)$		$\bar{w}(a/2,b/2\ \max)$	$\bar{\sigma}_{xx}(a/2,0,0\ \&\ h)$		$\bar{\sigma}_{yy}(0,b/2,0\ \&\ h)$		$\bar{\tau}_{xy}(a/2,b/2,0\ \&\ h)$		$\bar{\tau}_{xz}(a/2,b/2,\max)$	$\bar{\tau}_{yz}(a/2,b/2,\max)$
1.5	0	Model 1	-5.769	-0.890	-3.846	-0.593	0.152	-5.753	-0.471	-13.99	-00.705	-9.894	-0.281	1.268	0.845
		Model 2	-5.487	-8.529	-3.658	-5.686	-0.095	-6.989	-10.939	-14.83	-13.185	-9.409	-2.694	4.034	2.689
	1	Model 1	-4.999	-1.158	-3.333	-0.772	0.120	-9.117	-0.255	-16.26	-0.560	-8.57	-0.366	0.776	0.517
		Model 2	-7.191	-4.060	-4.794	-2.706	0.093	0.458	2.081	-9.818	1.012	-12.33	-1.282	10.156	6.771
	2	Model 1	-5.718	-1.992	-3.812	-1.328	0.114	-5.979	0.416	-14.15	-0.108	-9.805	-0.629	2.718	1.812
		Model 2	-7.372	-1.401	-4.914	-0.934	0.181	1.248	-0.059	-9.287	-0.428	-12.65	-0.443	7.214	4.809
	4	Model 1	-7.083	-2.645	-4.722	-1.763	0.133	-0.014	0.942	-10.14	0.246	-12.15	-0.836	6.512	4.341
		Model 2	-6.792	0.260	-4.528	0.173	0.220	-1.285	-1.396	-10.99	-1.328	-11.65	0.082	2.519	1.680
	8	Model 1	-8.908	-2.813	-5.939	-1.875	0.182	7.960	1.077	-4.770	0.336	-15.28	-0.888	8.934	5.956
		Model 2	-5.753	0.567	-3.836	0.378	0.202	-5.823	-1.643	-14.04	-1.494	-9.866	0.179	4.076	2.717
	10	Model 1	-9.529	-2.773	-6.352	-1.849	0.203	10.673	1.045	-02.944	0.315	-16.340	-0.876	8.907	5.938
		Model 2	-5.402	0.513	-3.601	0.342	0.190	-7.359	-1.600	-15.078	-1.465	-9.263	0.162	4.091	2.727
3.0	0	Model 1	-0.007	-0.001	-0.002	0.000	0.000	-0.013	-0.003	-0.192	-0.008	-0.064	-0.002	0.127	0.042
		Model 2	-0.007	-0.011	-0.002	-0.004	0.000	-0.031	-0.098	-0.192	-0.144	-0.060	-0.017	0.440	0.147
	1	Model 1	-0.007	-0.002	-0.002	-0.001	0.000	-0.052	-0.001	-0.155	-0.007	-0.056	-0.002	0.077	0.026
		Model 2	-0.009	-0.005	-0.003	-0.002	0.000	0.058	0.026	-0.155	0.004	-0.080	-0.008	0.990	0.330
	2	Model 1	-0.007	-0.003	-0.002	-0.001	0.000	-0.015	0.007	-0.150	-0.004	-0.064	-0.004	0.279	0.093
		Model 2	-0.010	-0.002	-0.003	-0.001	0.000	0.068	0.001	-0.150	-0.006	-0.082	-0.003	0.705	0.235
	4	Model 1	-0.009	-0.003	-0.003	-0.001	0.000	0.056	0.014	-0.163	-0.001	-0.079	-0.006	0.667	0.222
		Model 2	-0.009	0.000	-0.003	0.000	0.000	0.038	-0.015	-0.163	-0.013	-0.075	0.001	0.260	0.087
	8	Model 1	-0.012	-0.004	-0.004	-0.001	0.000	0.151	0.015	-0.185	-0.001	-0.100	-0.006	0.910	0.303
		Model 2	-0.007	0.001	-0.002	0.000	0.000	-0.015	-0.018	-0.185	-0.014	-0.064	0.001	0.414	0.138
	10	Model 1	-0.012	-0.004	-0.004	-0.001	0.000	0.183	0.015	-0.193	-0.001	-0.107	-0.006	0.907	0.302
		Model 2	-0.007	0.001	-0.002	0.000	0.000	-0.033	-0.017	-0.193	-0.014	-0.060	0.001	0.415	0.138

Table 10. Normalized in plane and transverse displacements $(\bar{u},\bar{v},\bar{w})$ and stresses $(\bar{\sigma}_{xx},\bar{\sigma}_{yy},\bar{\tau}_{xy},\bar{\tau}_{xz},\bar{\tau}_{yz})$ of Rectangular FG plate under bi-direction sinusoidal transverse loading for side to thickness ratio 5.0 for material set C

b/a	k	Model	$\bar{u}(a,0,0\ \&\ h)$		$\bar{v}(0,b,0\ \&\ h)$		$\bar{w}(a/2,b/2\ \max)$	$\bar{\sigma}_{xx}(a/2,0,0\ \&\ h)$		$\bar{\sigma}_{yy}(0,b/2,0\ \&\ h)$		$\bar{\tau}_{xy}(a/2,b/2,0\ \&\ h)$		$\bar{\tau}_{xz}(a/2,b/2,\max)$	$\bar{\tau}_{yz}(a/2,b/2,\max)$
1.5	0	Model 1	-8.714	-1.337	-5.797	-0.880	0.229	-0.908	-0.715	-2.206	-1.078	-1.561	-0.430	0.206	0.142
		Model 2	-7.918	-13.585	-5.252	-9.029	-0.178	-1.254	-15.774	-2.436	-19.430	-1.416	-4.393	1.918	1.277
	1	Model 1	-8.970	-0.524	-5.969	-0.339	0.263	-2.443	-0.734	-3.778	-0.878	-1.607	-0.167	1.100	0.742
		Model 2	-12.87	-2.190	-8.564	-1.443	0.333	-0.752	0.568	-2.669	-0.025	-2.306	-0.705	1.319	0.888
	2	Model 1	-9.404	-0.935	-6.257	-0.612	0.264	-2.255	-0.413	-3.655	-0.668	-1.685	-0.300	0.525	0.360
		Model 2	-11.19	0.114	-7.447	0.088	0.350	-1.481	-1.234	-3.147	-1.207	-2.005	0.040	1.441	0.969
	4	Model 1	-10.61	-1.290	-7.064	-0.847	0.290	-1.729	-0.135	-3.310	-0.486	-1.902	-0.415	0.311	0.218
		Model 2	-8.389	0.798	-5.584	0.540	0.285	-2.694	-1.769	-3.943	-1.557	-1.503	0.260	3.521	2.357
	8	Model 1	-12.30	-1.440	-8.186	-0.944	0.337	-0.998	-0.018	-2.831	-0.410	-2.204	-0.463	0.961	0.648
		Model 2	-5.663	0.436	-3.769	0.297	0.191	-3.875	-1.485	-4.718	-1.370	-1.015	0.143	3.504	2.343
	10	Model 1	-12.84	-1.443	-8.542	-0.946	0.354	-0.766	-0.016	-2.678	-0.409	-2.300	-0.463	1.089	0.734
		Model 2	-4.952	0.249	-3.296	0.171	0.164	-4.183	-1.339	-4.920	-1.273	-0.887	0.082	3.222	2.155
3.0	0	Model 1	-0.011	-0.002	-0.004	-0.001	0.000	-0.002	-0.005	-0.031	-0.013	-0.010	-0.003	0.021	0.007
		Model 2	-0.010	-0.018	-0.003	-0.006	0.000	-0.007	-0.139	-0.031	-0.214	-0.009	-0.028	0.197	0.066
	1	Model 1	-0.012	-0.001	-0.004	0.000	0.000	-0.017	-0.007	-0.037	-0.010	-0.010	-0.001	0.111	0.038
		Model 2	-0.017	-0.003	-0.006	-0.001	0.000	0.002	0.008	-0.037	-0.004	-0.015	-0.004	0.124	0.042
	2	Model 1	-0.012	-0.001	-0.004	0.000	0.000	-0.015	-0.003	-0.041	-0.008	-0.011	-0.002	0.052	0.019
		Model 2	-0.014	0.000	-0.005	0.000	0.000	-0.006	-0.013	-0.041	-0.012	-0.013	0.000	0.151	0.051
	4	Model 1	-0.014	-0.002	-0.005	-0.001	0.000	-0.008	0.001	-0.046	-0.007	-0.012	-0.003	0.033	0.012
		Model 2	-0.011	0.001	-0.004	0.000	0.000	-0.021	-0.019	-0.046	-0.015	-0.010	0.002	0.358	0.121
	8	Model 1	-0.016	-0.002	-0.005	-0.001	0.000	0.000	0.002	-0.052	-0.006	-0.014	-0.003	0.099	0.034
		Model 2	-0.007	0.001	-0.002	0.000	0.000	-0.034	-0.016	-0.052	-0.013	-0.007	0.001	0.355	0.119
	10	Model 1	-0.017	-0.002	-0.006	-0.001	0.000	-0.037	-0.006	-0.053	-0.006	-0.015	-0.003	0.112	0.038
		Model 2	-0.006	0.000	-0.002	0.000	0.000	-0.038	-0.014	-0.053	-0.012	-0.006	0.001	0.326	0.109

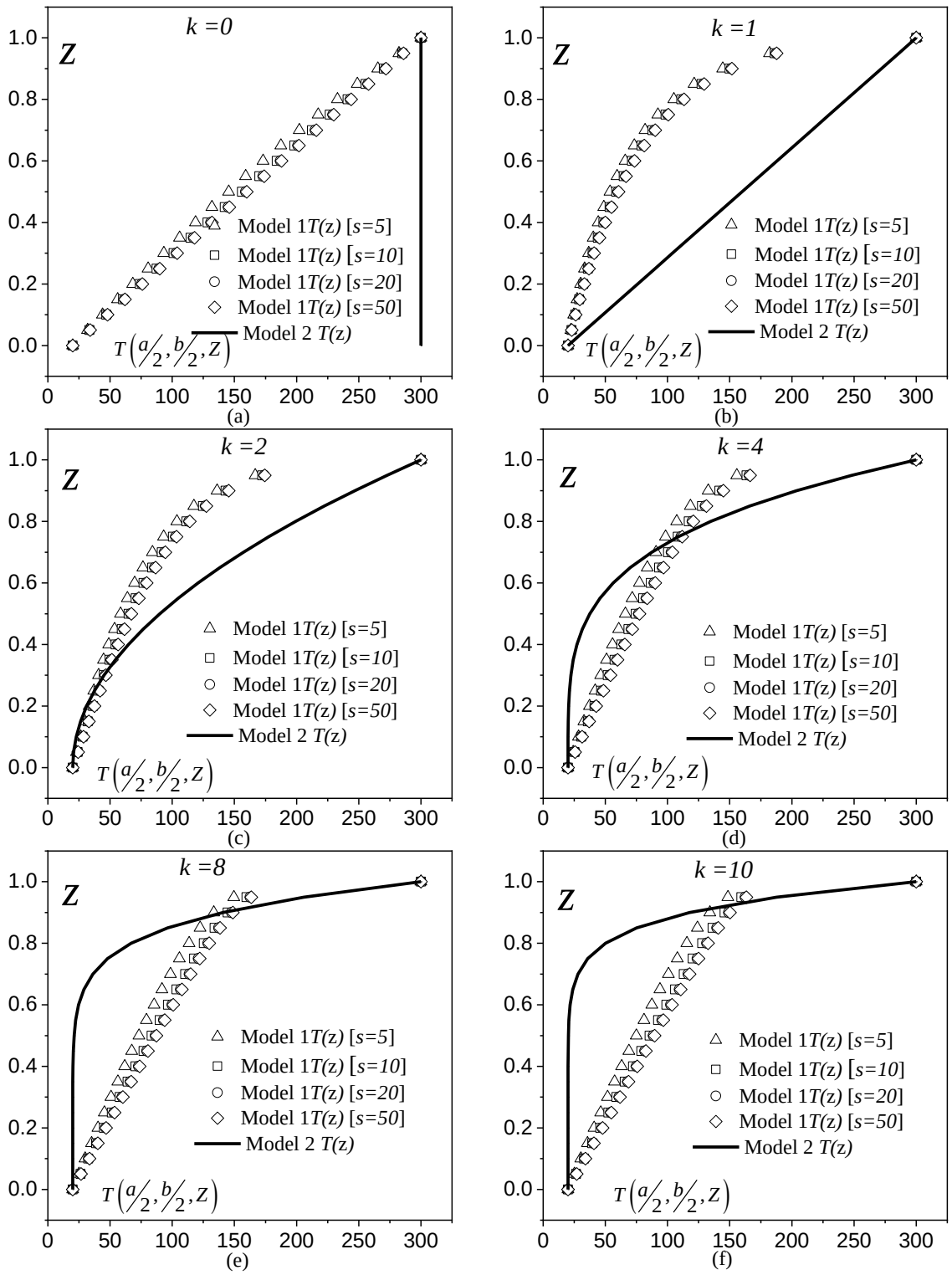

Fig. 2. Comparison between through thickness exact temperature variation and power law variation for different power index (*k*) for square laminate material set A.

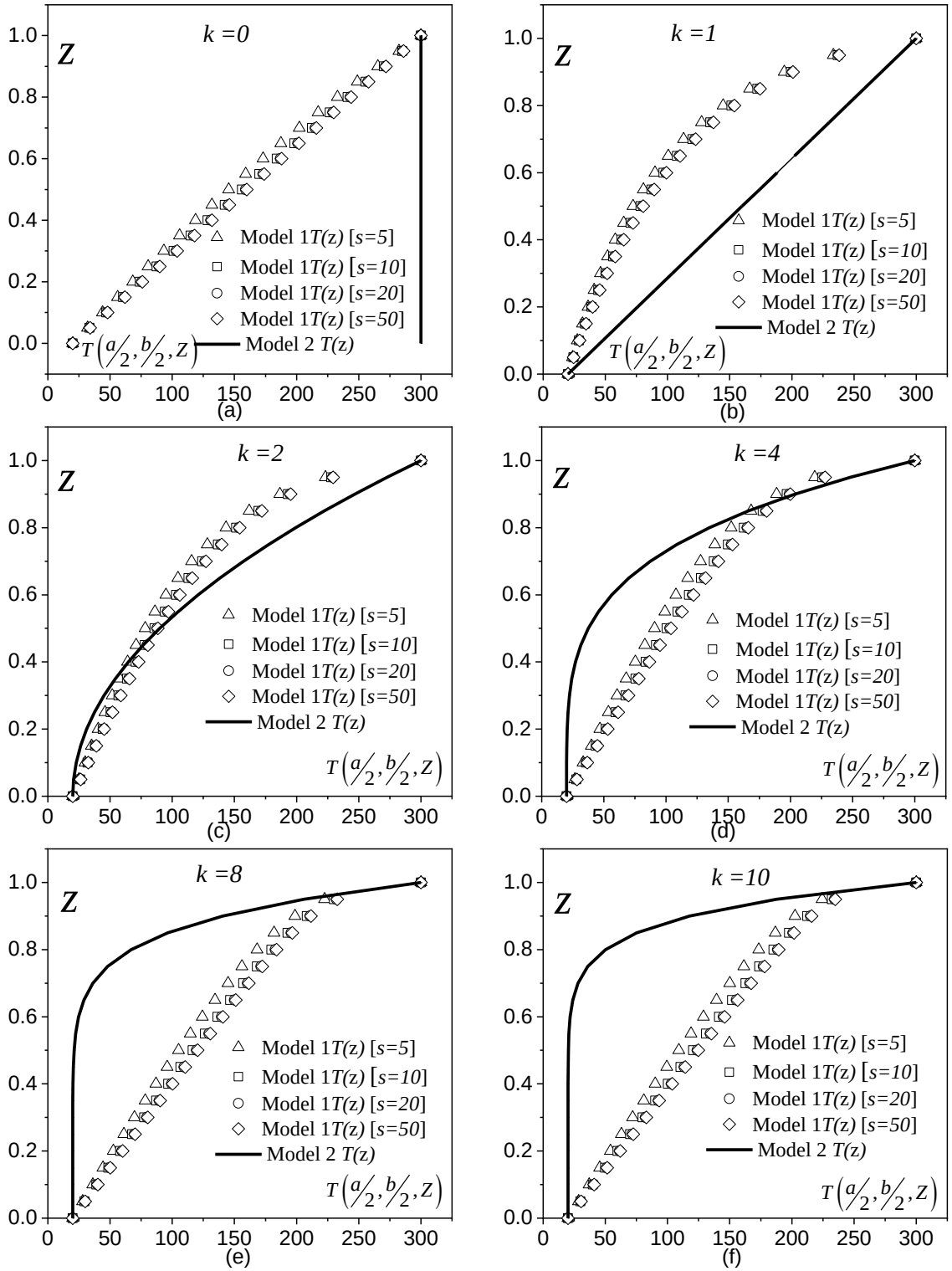

Fig. 3. Comparison between through thickness exact temperature variation and power law variation for different power index (*k*) for square laminate material set B.

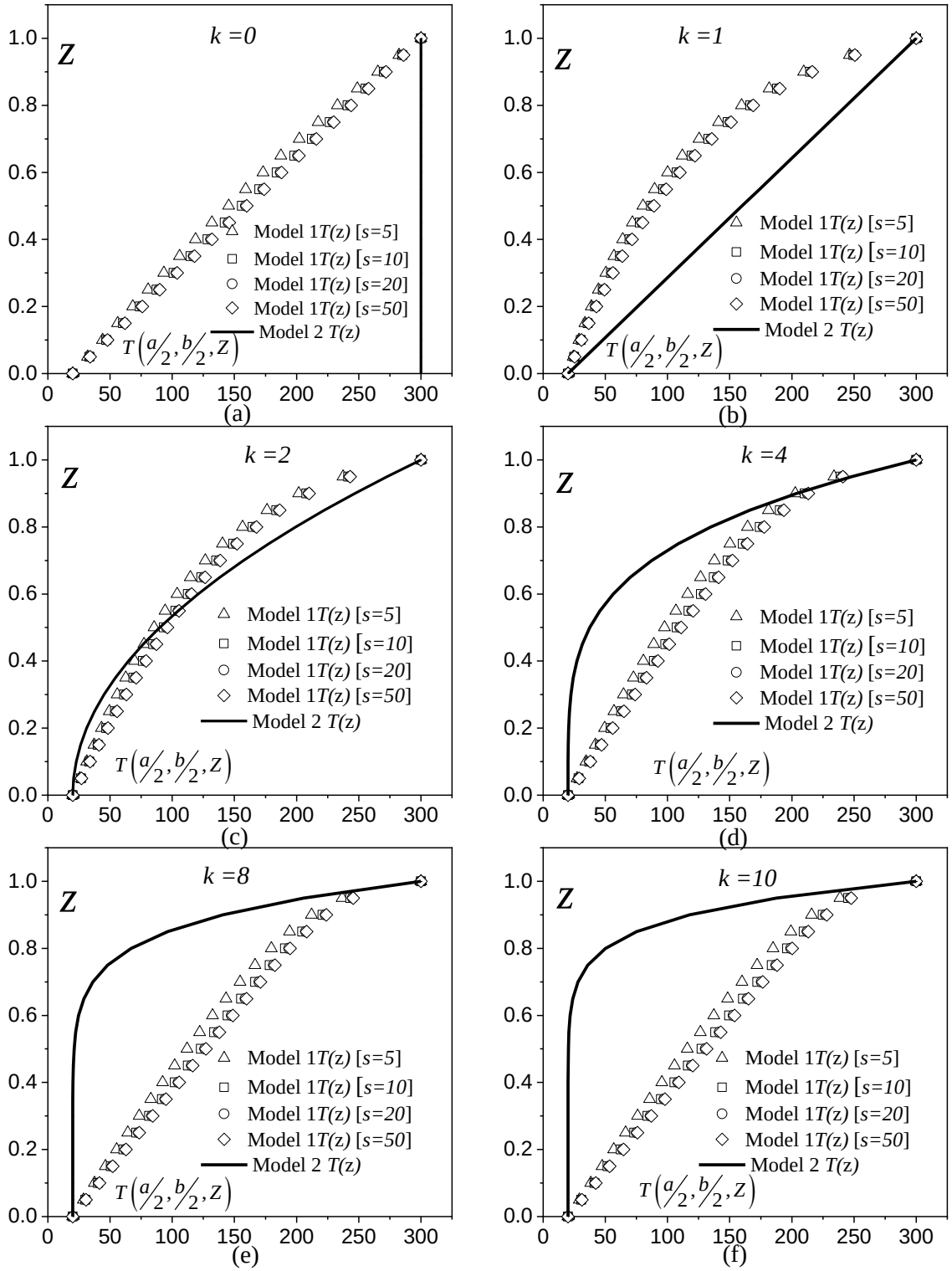

Fig. 4. Comparison between through thickness exact temperature variation and power law variation for different power index (*k*) for square laminate material set C.

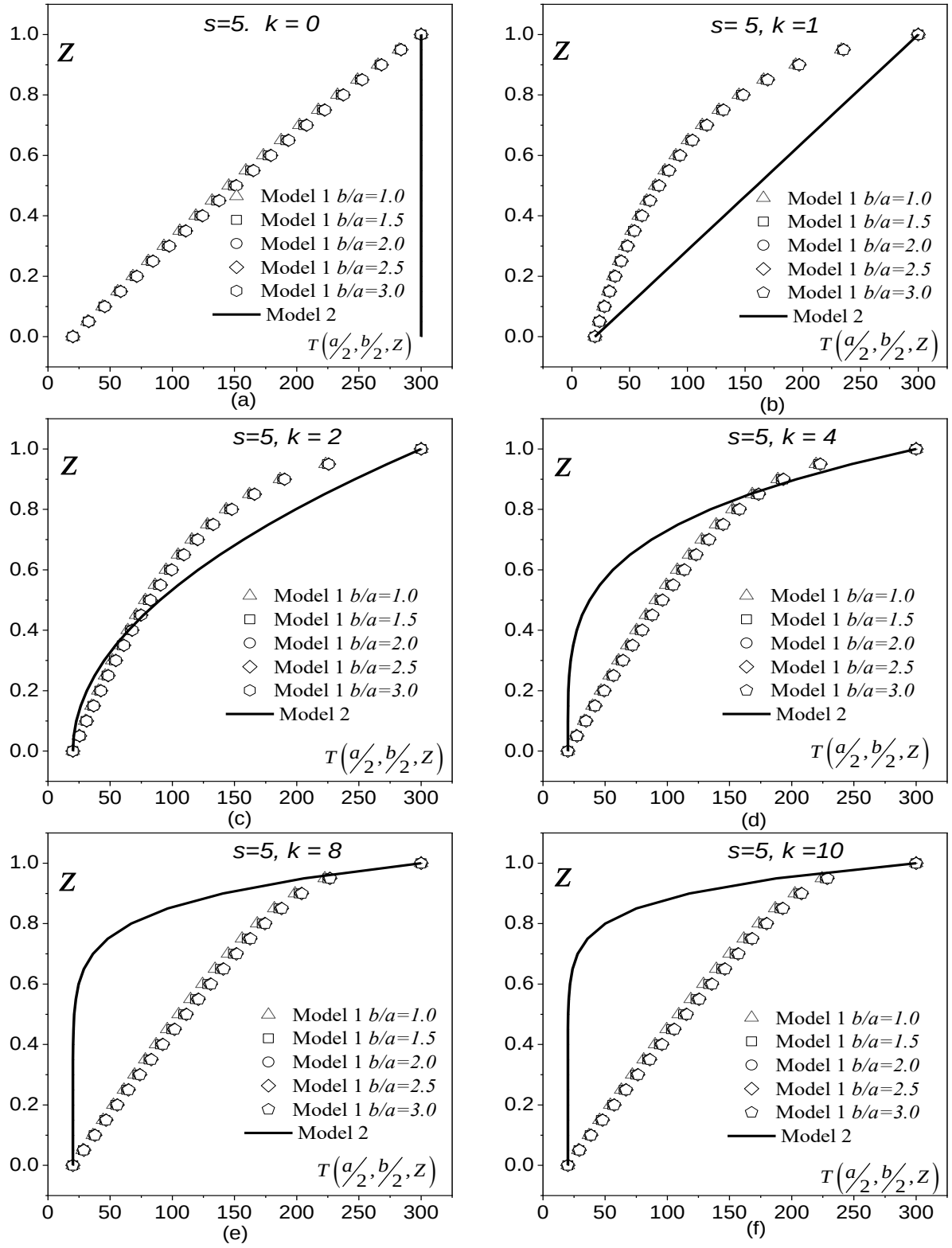

Fig. 5. Comparison between through thickness exact temperature variation and power law variation for different power index (*k)* for square laminate (*b/a*=1) and rectangular laminate (*b/a*=1.5,2.0,2.5,3.0) material set B.

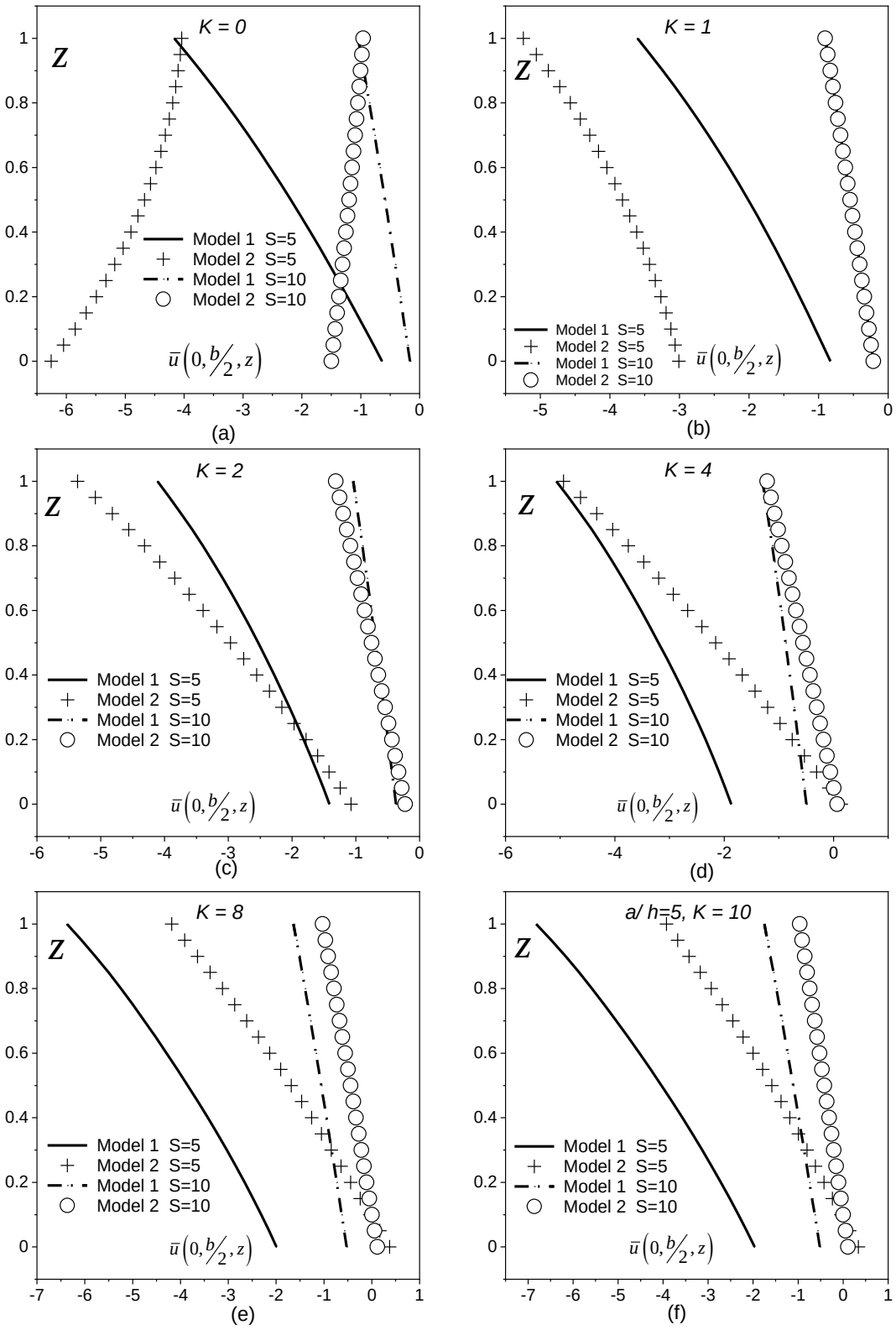

Fig. 6. Thickness variation of normalized in plane displacement ($\bar{u}$) for different material graded FG square laminate for material set B.

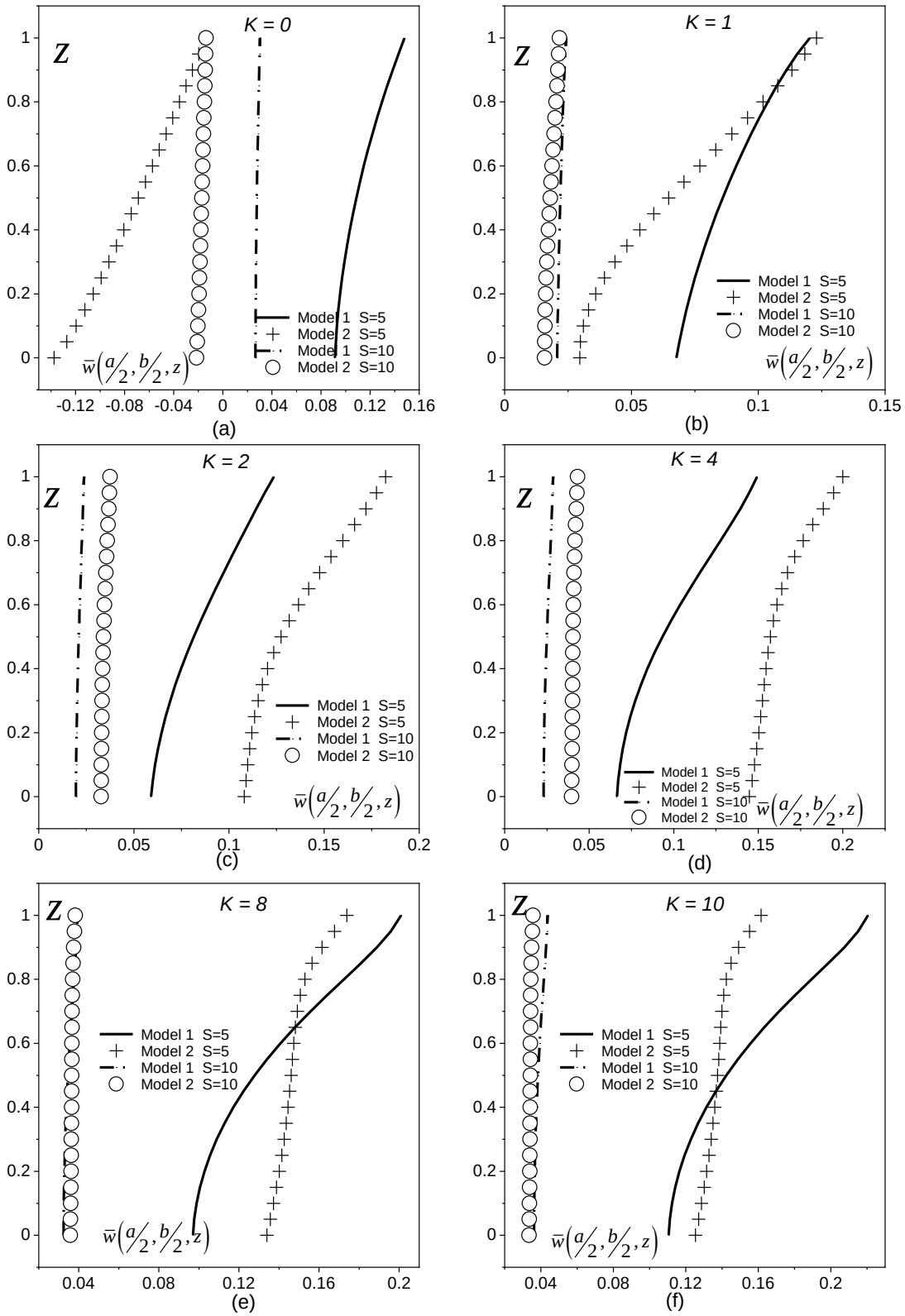

Fig. 7. Thickness variation of normalized Transverse displacement ($\bar{w}$) for different material graded FG square laminate for material set B.

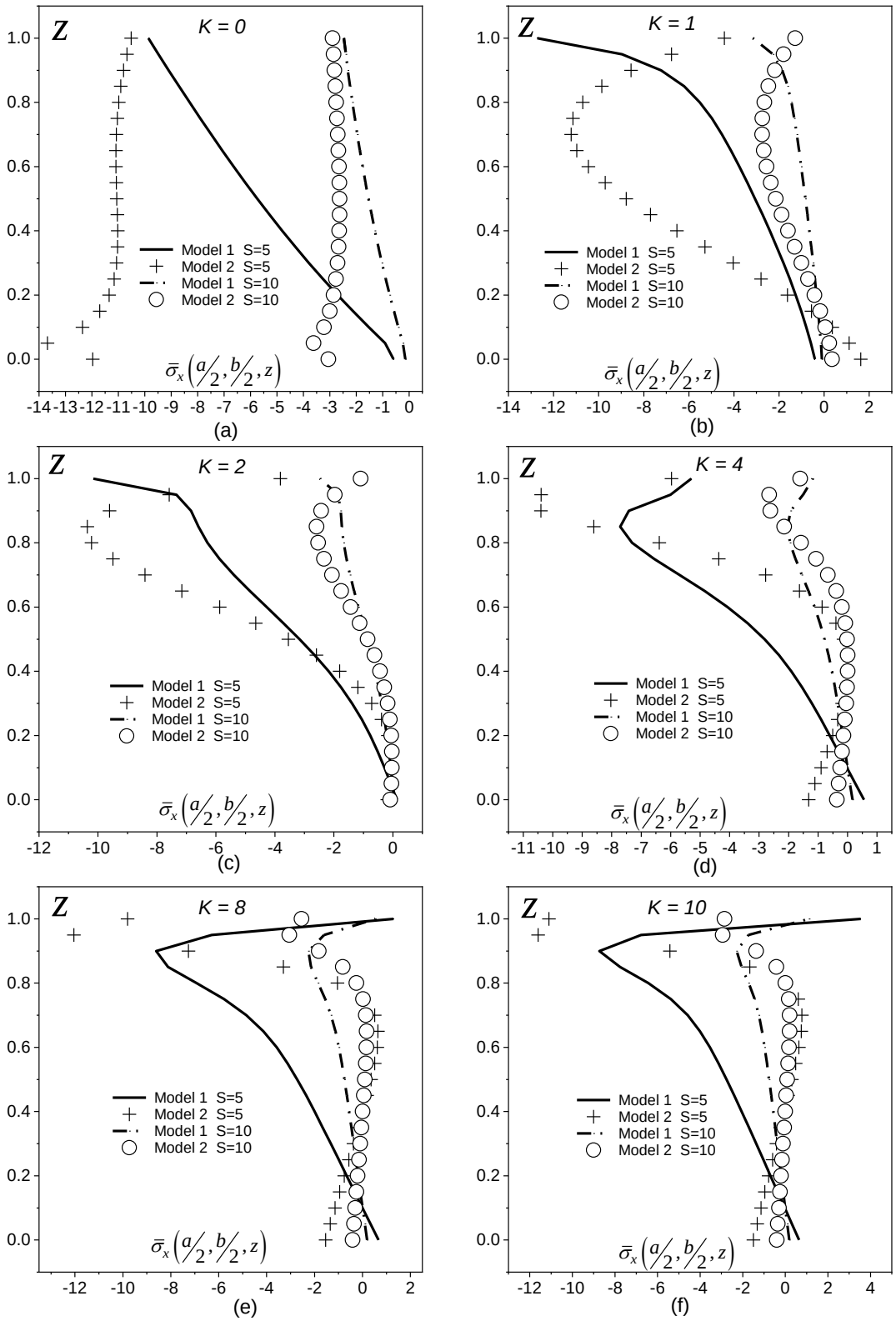

Fig. 8. Thickness variation of normalized Transverse displacement ($\bar{\sigma}_x$) for different material graded FG square laminate for material set B.

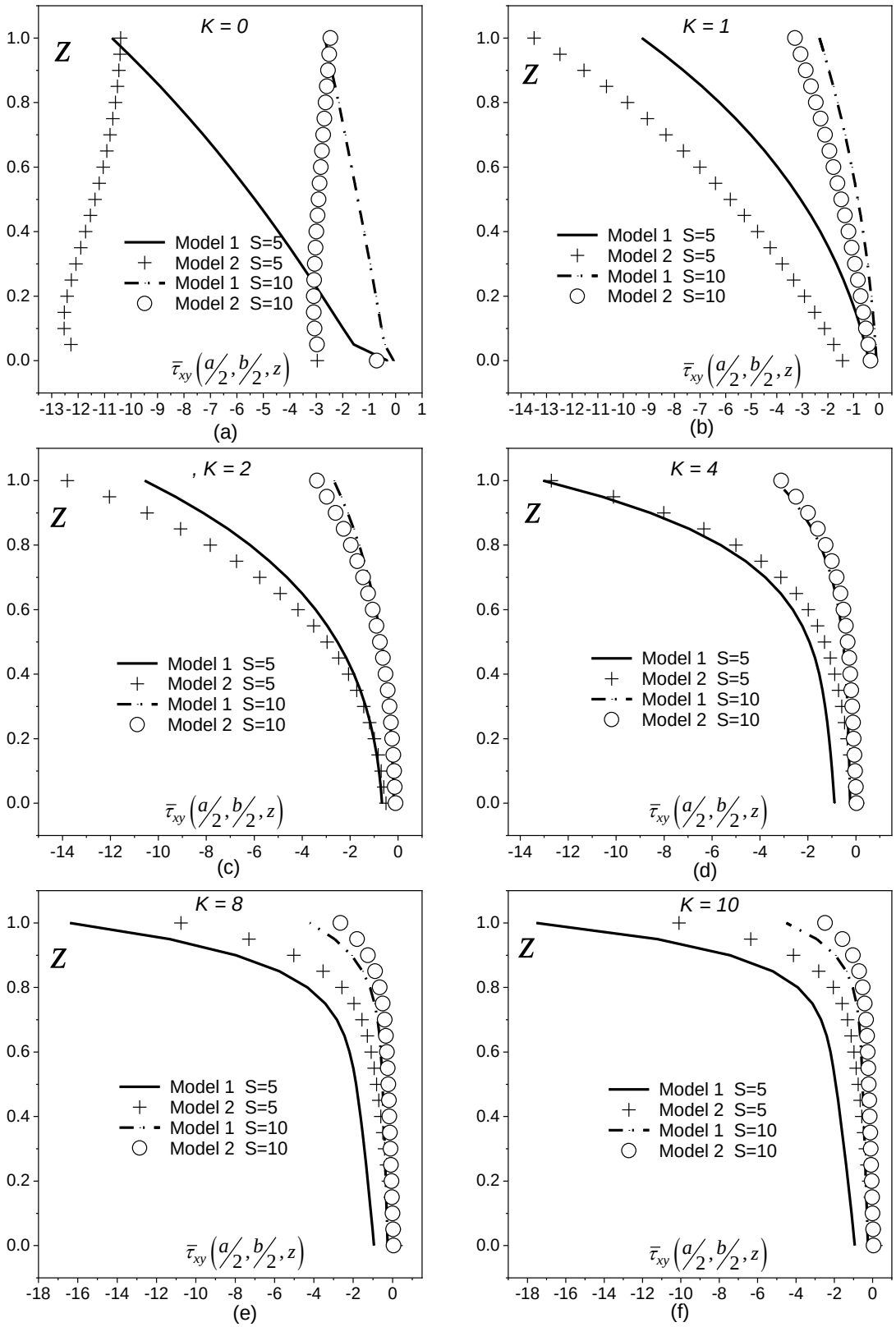

Fig. 9. Thickness variation of normalized Transverse displacement ($\bar{\tau}_{xy}$) for different material graded FG square laminate for material set B.

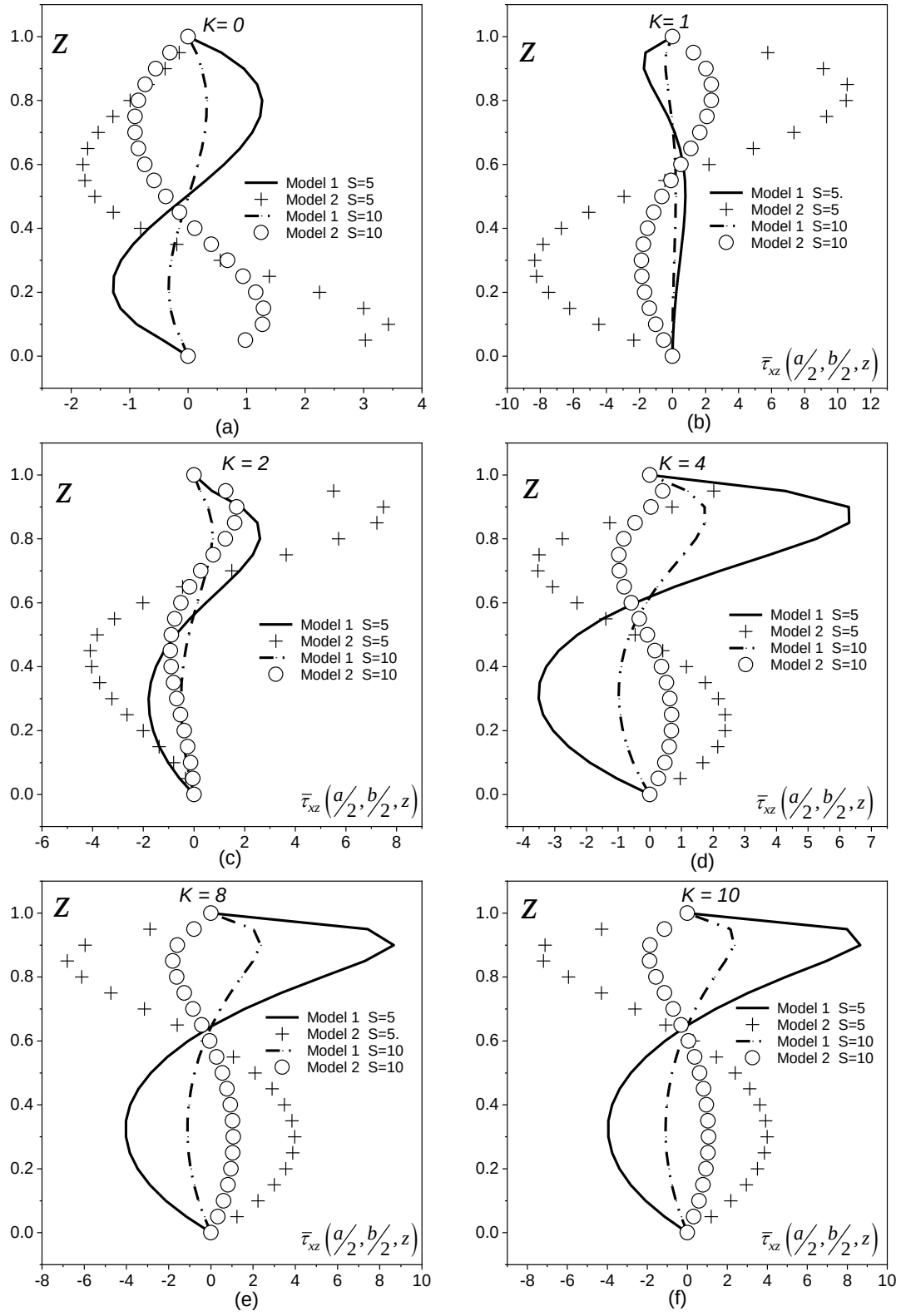

Fig. 10. Thickness variation of normalized Transverse displacement ($\bar{\tau}_{xz}$) for different material graded FG square laminate for material set B.

6. Concluding remarks

This paper attempts to capture the actual temperature profile through the laminate thickness due to the heat conduction formulation. Here temperature causing stress analysis has been performed for both exact temperature profile and power law varying temperature profile with the semi-analytical formulation. This semi-analytical formulation discussed here has based on a two-point boundary value problem (BVP), which has depended on first-order differential equations (ODE's). Comparison between exact and assumed temperature profiles had been documented for various material sets, different aspect ratios, different power indices (k), and width to length ratios changing from thick to thin, square to rectangular laminate. In the current study, the material property's effect has been noted on the thermal profile, whereas the aspect ratio does not impact it. From the thermal stress analysis, it has to be noted that the exact determination of thermal profile is of utmost importance since material property, aspect ratios, power indexes (k), etc., parameters have a specific impact on stress analysis. A significant difference in numerical results between thermal stress analyses was observed for exact and assumed temperature profiles. The semi-analytical approach presented here has the advantage of both analytical and numerical methods, which help achieve simplicity and accuracy simultaneously, leading to avoiding complex 3D solutions. The present formulation is capable of handling only all-around simply supported laminate subjected to only distributed loading. In the future, the presented formulation can be possible to extend for FG laminates with various boundary conditions, multidimensional volume fraction change etc. Also, it is possible to handle other smart materials like a composite, sandwich, piezoelectric materials, etc., after few mathematical manipulations within the presented formulation.

References

[1] Vel SS, Batra RC. Three-dimensional analysis of transient thermal stresses in functionally graded plates. Int J Solids Struct 2003;40:7181–96. https://doi.org/10.1016/S0020-7683(03)00361-5.

[2] Javaheri R, Eslami MR. Thermal Buckling of Functionally Graded Plates Based on Higher-Order Theory. J Therm Stress 2002;25:603–25. https://doi.org/10.1080/01495730290074333.

[3] Ghannadpour SAM, Ovesy HR, Nassirnia M. Buckling analysis of functionally graded plates under thermal loadings using the finite strip method. Comput Struct 2012;108–109:93–9. https://doi.org/10.1016/j.compstruc.2012.02.011.

[4] Damanpack AR, Bodaghi M, Ghassemi H, Sayehbani M. Boundary element method applied to the bending analysis of thin functionally graded plates. Lat Am J Solids Struct 2013;10:549–70.

[5] Shen H-S. Nonlinear bending response of functionally graded plates subjected to transverse loads and in thermal environments. Int J Mech Sci 2002;44:561–84. https://doi.org/10.1016/S0020-7403(01)00103-5.

[6] Lanhe W. Thermal buckling of a simply supported moderately thick rectangular FGM

plate. Compos Struct 2004;64:211–8. https://doi.org/10.1016/j.compstruct.2003.08.004.

[7] Dai KY, Liu GR, Han X, Lim KM. Thermomechanical analysis of functionally graded material (FGM) plates using element-free Galerkin method. Comput Struct 2005;83:1487–502. https://doi.org/10.1016/j.compstruc.2004.09.020.

[8] Nguyen T-K, Sab K, Bonnet G. First-order shear deformation plate models for functionally graded materials. Compos Struct 2008;83:25–36. https://doi.org/10.1016/j.compstruct.2007.03.004.

[9] Yang J, Shen H-S. Nonlinear bending analysis of shear deformable functionally graded plates subjected to thermo-mechanical loads under various boundary conditions. Compos Part B Eng 2003;34:103–15. https://doi.org/10.1016/S1359-8368(02)00083-5.

[10] Zenkour AM. Generalized shear deformation theory for bending analysis of functionally graded plates. Appl Math Model 2006;30:67–84. https://doi.org/10.1016/j.apm.2005.03.009.

[11] Saidi AR, Jomehzadeh E. On the analytical approach for the bending/stretching of linearly elastic functionally graded rectangular plates with two opposite edges simply supported. Proc Inst Mech Eng Part C J Mech Eng Sci 2009;223:2009–16. https://doi.org/10.1243/09544062JMES1431.

[12] Kadoli R, Akhtar K, Ganesan N. Static analysis of functionally graded beams using higher order shear deformation theory. Appl Math Model 2008;32:2509–25. https://doi.org/10.1016/j.apm.2007.09.015.

[13] Mantari JL, Oktem AS, Guedes Soares C. Bending response of functionally graded plates by using a new higher order shear deformation theory. Compos Struct 2012;94:714–23. https://doi.org/10.1016/j.compstruct.2011.09.007.

[14] Kant T, Jha DK, Singh RK. A higher-order shear and normal deformation functionally graded plate model: some recent results. Acta Mech 2014;225:2865–76. https://doi.org/10.1007/s00707-014-1213-2.

[15] Ferreira AJM, Roque CMC, Jorge RMN, Fasshauer GE, Batra RC. Analysis of Functionally Graded Plates by a Robust Meshless Method. Mech Adv Mater Struct 2007;14:577–87. https://doi.org/10.1080/15376490701672732.

[16] Akbarzadeh AH, Zad SKH, Eslami MR, Sadighi M. Mechanical behaviour of functionally graded plates under static and dynamic loading. Proc Inst Mech Eng Part C J Mech Eng Sci 2011;225:326–33. https://doi.org/10.1243/09544062JMES2111.

[17] Wu C-P, Li H-Y. An RMVT-based third-order shear deformation theory of multilayered functionally graded material plates. Compos Struct 2010;92:2591–605. https://doi.org/10.1016/j.compstruct.2010.01.022.

[18] Xiang S, Kang G. A nth-order shear deformation theory for the bending analysis on the functionally graded plates. Eur J Mech - A/Solids 2013;37:336–43. https://doi.org/10.1016/j.euromechsol.2012.08.005.

[19] Tounsi A, Al-Dulaijan SU, Al-Osta MA, Chikh A, Al-Zahrani MM, Sharif A, et al. A four variable trigonometric integral plate theory for hygro-thermo-mechanical bending analysis of AFG ceramic-metal plates resting on a two-parameter elastic foundation. Steel Compos

Struct 2020;34:511–24.

[20] Chikr SC, Kaci A, Bousahla AA, Bourada F, Tounsi A, Bedia EA, et al. A novel four-unknown integral model for buckling response of FG sandwich plates resting on elastic foundations under various boundary conditions using Galerkin's approach. Geomech Eng 2020;21:471–87.

[21] Refrafi S, Bousahla AA, Bouhadra A, Menasria A, Bourada F, Tounsi A, et al. Effects of hygro-thermo-mechanical conditions on the buckling of FG sandwich plates resting on elastic foundations. Comput Concr 2020;25:311–25.

[22] Boussoula A, Boucham B, Bourada M, Bourada F, Tounsi A, Bousahla AA, et al. A simple nth-order shear deformation theory for thermomechanical bending analysis of different configurations of FG sandwich plates. Smart Struct Syst 2020;25:197–218.

[23] Balubaid M, Tounsi A, Dakhel B, Mahmoud SR. Free vibration investigation of FG nanoscale plate using nonlocal two variables integral refined plate theory. Comput Concr 2019;24:579–86.

[24] Kaddari M, Kaci A, Bousahla AA, Tounsi A, Bourada F, Tounsi A, et al. A study on the structural behaviour of functionally graded porous plates on elastic foundation using a new quasi-3D model: bending and free vibration analysis. Comput Concr 2020;25:37–57.

[25] Roy AM. Barrierless melt nucleation at solid-solid interface in energetic nitramine octahydro-1, 3, 5, 7-tetranitro-1, 3, 5, 7-tetrazocine. Materialia 2021;15:101000. https://doi.org/10.1016/j.mtla.2021.101000.

[26] Smilowitz L, Henson BF, Asay BW, Dickson PM. The β–δ phase transition in the energetic nitramine-octahydro-1,3,5,7-tetranitro-1,3,5,7-tetrazocine: Kinetics. J Chem Phys 2002;117:3789–98. https://doi.org/10.1063/1.1495399.

[27] Henson BF, Smilowitz L, Asay BW, Dickson PM. The β–δ phase transition in the energetic nitramine octahydro-1,3,5,7-tetranitro-1,3,5,7-tetrazocine: Thermodynamics. J Chem Phys 2002;117:3780–8. https://doi.org/10.1063/1.1495398.

[28] Bowlan P, Henson BF, Smilowitz L, Levitas VI, Suvorova N, Oschwald D. Kinetics of the γ–δ phase transition in energetic nitramine-octahydro-1,3,5,7-tetranitro-1,3,5,7-tetrazocine. J Chem Phys 2019;150:064705. https://doi.org/10.1063/1.5080010.

[29] Levitas VI, Henson BF, Smilowitz LB, Asay BW. Solid-Solid Phase Transformation via Virtual Melting Significantly Below the Melting Temperature. Phys Rev Lett 2004;92:235702. https://doi.org/10.1103/PhysRevLett.92.235702.

[30] Pendhari SS, Kulkarni SP. Cylindrical Bending of Power Law Varied Functionally Graded Laminate Subjected to Thermo-Mechanical Loading. Comput Eng Phys Model 2020;3:22–46. https://doi.org/10.22115/cepm.2020.243741.1124.

[31] Kantorovich LV. Approximate methods of higher analysis. Interscience 1958.